A Commutation Failure Prediction and Mitigation Method

Renlong Zhu, Xiaoping Zhou, Haitao Xia, Lerong Hong, and Hanhang Yin

Abstract—The mitigation of commutation failure (CF) depends on the accuracy of CF prediction. In terms of the large error of the existing extinction angle (EA) calculation during the fault transient period, a method for CF prediction and mitigation is proposed. Variations in both DC current and overlap angle (OA) are considered in the proposed method to predict the EA rapidly. In addition, variations in critical EA and the effect of firing angle (FA) on both DC current and OA are considered in the proposed method to obtain the accurate FA order for the control system. The proposed method can achieve good performance in terms of CF mitigation and reduce reactive consumption at the inverter side when a fault occurs. Simulation results based on the PSCAD/EMTDC show that the proposed method predicts CF rapidly and exhibits good performance in terms of CF mitigation.

Index Terms—Commutation failure prediction, commutation failure mitigation, line commutated converter based high-voltage direct current (LCC-HVDC), extinction angle (EA), overlap angle (OA), firing angle (FA).

I. INTRODUCTION

LINE commutated converted based high-voltage direct current (LCC-HVDC) systems are widely applied owing to the geographical separation of primary energy resources and load centers [1] - [3]. Compared with the voltage-source-converter-based high-voltage direct current (VSC-HVDC) systems, LCC-HVDC systems are advantageous in terms of capital cost and power loss [4]. However, commutation failure (CF) at the inverter side is an adverse and frequent dynamic event in LCC-HVDC systems [5].

CF occurs when a thyristor valves, which is supposed to be turned off, and continues to conduct the electricity without transferring its current to the next valve in the firing sequence [6]. The CF can cause stress increment in devices and interruptions in the transmitted power [7]. In particular, repeated CFs might result in the outage of the LCC-HVDC system or severe cascading failures [8], [9]. Most CFs are caused by AC voltage disturbances such as AC voltage reduction, phase shift with asymmetrical faults, and AC voltage distortion caused by harmonics [10], [11]. Since AC voltage disturbance cannot be completely avoided, the methods for predicting CF and corrective measures for mitigating CF must be identified and developed, respectively.

To date, many solutions have been proposed to reduce the risk of CF, and they can be classified into three categories. The main idea of the first category is to integrate additional capacitive elements into the inverter, e.g., a capacitor-commutated converter (CCC) [12], [13], a controlled series capacitor converter [14], an evolved CCC embedded with an anti-parallel thyristor-based dual-directional full-bridge module, and an enhanced line commutated converter (LCC) integrated with a thyristor-based full-bridge module [15]. The additional capacitive elements provide additional commutation voltage-time area by compensating the valve commutation voltage and thus prevent CF. However, the additional capacitive elements will increase the cost and complicate the control system. The main idea of the second category is to use additional devices. The utilization of reactive power compensators such as static var compensator (SVC) and static compensator (STATCOM) at the inverter side to regulate the AC voltage can be effective in mitigating repeated CFs [16], [17]. However, the cost will be increased. In addition, CF can be effectively prevented by equipping a DC chopper at the DC terminal of the inverter [18] and a superconducting fault current limiter on the inverter-side AC bus [19]. However, current limiters are expensive and not yet applied extensively.

The main idea of the third category is to modify the control of LCC-HVDC systems. The voltage-dependent current order limiter (VDCOL) and the improved VDCOL [20], [21] have been widely used in LCC-HVDC systems to reduce the risk of CF and improve fault recovery performance, whereas the transmission delay of the DC current order from the inverter to the rectifier restricts the capability of the first CF mitigation. Reference [22] proposes commutation failure prevention (CFPREV) control to mitigate CF by immediately advancing the firing angle (FA) when AC faults are detected. However, the CF mitigation performance of the CFPREV control requires an improvement via parameter tuning. Reference [23] proposes a predictive extinction angle (EA) control method that considers the changes in the DC. However, the overlap angle (OA) is overestimated and the reactive consumption increases unnecessarily. Reference [24] proposes a

R. Zhu, X. Zhou (corresponding author), H. Xia, L. Hong, and H. Yin are with the College of Electrical and Information Engineering, Hunan University, Changsha 410082, China (e-mail: 635107372@qq.com; zxp2011@hnu.edu.cn; xht0903@163.com; hlr0908@163.com; 296262037@qq.com).

DC current predictive control strategy for CF mitigation. However, the delay of communication between the inverter and rectifier sides as well as the lag of DC current control is disregarded. Reference [25] proposes an enhanced strategy to inhibit CF using the triangle similarity theorem to approximate the overlap area. However, the error of the triangle approximation for determining the FA is not negligible, whereas the DC current change of the next commutation process is disregarded. Reference [26] proposes a method to calculate the pseudo-EA that enables real-time EA calculation. However, the FA update in [25] is the same as the measured EA update, and the pseudo-EA update in [26] is the same as the pseudo-commutation voltage crosses zero, which causes a control delay in the FA control and may undermine the performance of CF mitigation. Although various methods have been proposed for mitigating CF, further improvements should be realized.

Herein, a method for CF prediction and mitigation is proposed. Based on the boundary condition of the commutation process and the DC current prediction, a method to predict the EA is proposed while considering the variations in the DC current and OA. An improved FA control strategy is proposed considering the variation in the critical EA and the effect of firing time on both the DC current and OA to provide a more accurate FA order prior to every commutation process. An accurate FA order prevents CF and minimizes reactive power consumption simultaneously.

The remainder of this paper is organized as follows. In Section II, the analysis of traditional calculations of EA and FA is discussed. Section III describes the methods for CF prediction and mitigation. In Section IV, several simulations of the CIGRE benchmark HVDC model are presented to verify the effectiveness of the proposed method. Finally, Section V concludes the paper.

II. TRADITIONAL CALCULATIONS OF EA AND FA

The basic module of a high-voltage direct current (HVDC) converter is a Graetz bridge, as shown in Fig. 1.
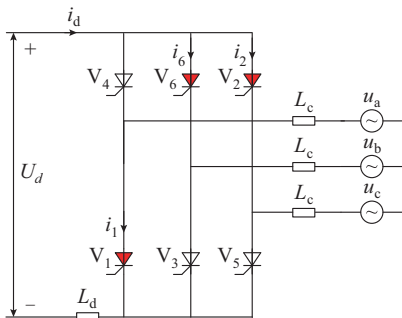

Fig. 1. Graetz bridge at inverter side.

The commutation from one valve to the next in the same row requires a certain time/electric angle, i.e., the commutation time/OA. In addition, the successful switching of a valve requires a certain time/electric angle, i.e., the deionization time/EA, to eliminate the internal stored charge produced during its forward conduction interval [25].

During the commutation process from valve 6 (V_6) to valve 2 (V_2), the circuit can be expressed as:

$$u_b + L_c \frac{di_6}{dt} = u_c + L_c \frac{di_2}{dt} \quad (1)$$

where L_c is the equivalent commutation inductance; u_b and u_c are the AC phase voltages; and i_2 and i_6 are the currents flowing through V_2 and V_6, respectively.

Equation (1) can be expressed as:

$$u_b - u_c = L_c \left(\frac{di_2}{dt} - \frac{di_6}{dt} \right) \quad (2)$$

Assuming $u_{bc} = \sqrt{2} E \sin(\omega t)$, where E is the root mean square (RMS) of AC line-to-line voltage and u_{bc} is the commutation voltage, the commutation process can be expressed as:

$$\sqrt{2} E \int_{\alpha}^{\alpha+\mu} \sin(\omega t) d(\omega t) = L_c \int_{\alpha}^{\alpha+\mu} \left(\frac{di_2}{dt} - \frac{di_6}{dt} \right) d(\omega t) \quad (3)$$

where α is the FA; and μ is the OA. Because $i_d = i_2 + i_6$ during the commutation, (3) can be expressed as:

$$\sqrt{2} E(\cos\alpha - \cos(\alpha+\mu)) = X_c (I_d(\alpha) + I_d(\alpha+\mu)) \quad (4)$$

where $X_c = \omega L_c$; and $I_d(\alpha)$ and $I_d(\alpha+\mu)$ are the DC currents at the start and end time instants of the commutation process, respectively. The left side of (4) is denoted by A_{fact}, i.e., the factual voltage-time area provided by the AC voltage. The right side of (4) is denoted by A_{de}, i.e., the demand voltage-time area for the commutation process.

Substituting $\alpha + \mu + \gamma = \pi$ into (4), EA can be calculated as:

$$\gamma = \arccos\left(X_c \frac{I_d(\alpha) + I_d(\alpha+\mu)}{\sqrt{2} E} - \cos\alpha \right) \quad (5)$$

Considering the phase shift in the commutation voltage $\Delta\varphi$, (4) can be rewritten as:

$$\gamma = \arccos\left(X_c \frac{I_d(\alpha) + I_d(\alpha+\mu)}{\sqrt{2} E} - \cos\alpha \right) - \Delta\varphi \quad (6)$$

Substituting $\gamma = \gamma_{ref}$ into (5), the FA can be calculated as:

$$\alpha = \arccos\left(X_c \frac{I_d(\alpha) + I_d(\alpha+\mu)}{\sqrt{2} E} - \cos\gamma_{ref} \right) \quad (7)$$

In the strategy of [25], the FA order of the constant EA controller is calculated as:

$$\alpha = \arccos\left(\frac{\sqrt{2} X_c I_d}{E} + k(I_{ord} - I_d) - \cos\gamma_{ref} \right) \quad (8)$$

where I_{ord} is the DC current order after VDCOL; and k is the correction coefficient ($k > 0$). Compared with (7), the additional term in (8) is $k(I_{ord} - I_d)$, which results in a positive slope for the inverter U_D and I_D (DC voltage and DC current) characteristics of the inverter. However, in this strategy, variations in the DC current and OA during the commutation are not considered accurately.

Considering the phase shift in the commutation voltage $\Delta\varphi$, (7) can be rewritten as:

$$\alpha = \arccos\left(X_c \frac{I_d(\alpha) + I_d(\alpha+\mu)}{\sqrt{2} E} - \cos(\gamma_{ref} + \Delta\varphi) \right) \quad (9)$$

Based on (6) and (9), the calculations of EA and FA de-

pend on the equivalent commutation inductance, RMS AC line-to-line voltage, OA, DC currents at the start and end time instants of the commutation process, and commutation voltage phase shift. In addition, the calculation of EA is affected by the FA order, and the calculation of the FA order is related to the EA reference value. The FA order determines the DC currents at the start and end time instants of the commutation process and OA. The OA is affected by the DC current at the end of the commutation process. Hence, the mutual effect among the DC current, FA, and OA must be considered in EA prediction and FA order calculations.

III. PROPOSED METHOD

The inductance at the DC side and inverter-side AC transmission lines enables the DC to change smoothly between the fault initial time instant and CF time instant. Therefore, the DC current can be predicted within a short time prior to CF based on the DC current and rate of change of the DC current. The DC current prediction can be expressed as:

$$I_{\text{dpre}}(\omega t) = I_{\text{d}}(\omega t_{\text{k}}) + (\omega t - \omega t_{\text{k}}) k_{I_{\text{d}}}(\omega t_{\text{k}}) \qquad (10)$$

where t_{k} is any sample time after the fault; $I_{\text{dpre}}(\omega t)$ and $I_{\text{d}}(\omega t_{\text{k}})$ are the predicted DC current at time t and the DC current at time t_{k}, respectively; and $k_{I_{\text{d}}}(\omega t_{\text{k}})$ is the rate of change of the DC current at time t_{k}. The prediction of the DC current becomes inaccurate after a CF occurs. However, the prediction is practical during the transient fault period before a CF occurs.

A. Prediction of EA

Figure 2 shows the commutation voltage and the relationship among the FA, predicted OA, and predicted EA at time t_{k}, where $E(\omega t_{\text{k}})$ is the RMS of AC line-to-line voltage at time t_{k}; μ_{pre} is the predicted OA at time t_{k}; and γ_{pre} is the predicted EA at time t_{k}.
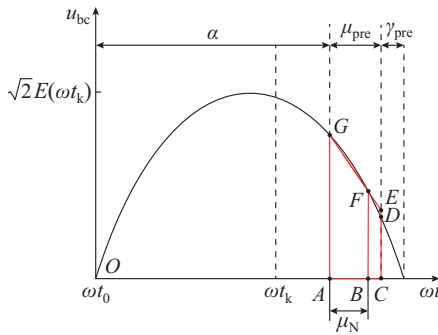

Fig. 2. Prediction of EA.

Based on Fig. 2, (4) can be rewritten as:

$$\sqrt{2}\, E(\omega t_{\text{k}})(\cos \alpha - \cos(\alpha + \mu_{\text{pre}})) = X_{\text{c}}(I_{\text{dpre}}(\alpha) + I_{\text{dpre}}(\alpha + \mu_{\text{pre}})) \qquad (11)$$

Substituting (10) into (11), we can obtain:

$$\sqrt{2}\, E(\omega t_{\text{k}})(\cos \alpha - \cos(\alpha + \mu_{\text{pre}})) = $$
$$X_{\text{c}}\{2I_{\text{d}}(\omega t_{\text{k}}) + [2\omega(t_0 - t_{\text{k}}) + 2\alpha + \mu_{\text{pre}}]k_{I_{\text{d}}}(\omega t_{\text{k}})\} \qquad (12)$$

where t_0 is the time when u_{bc} changes from negative to posi-

tive. The left side of (12), which is the factual voltage-time area A_{fact}, is equal to the area of the curved trapezoid *ACDG* shown in Fig. 2. The accurate value of A_{fact} can be calculated using the left side of (12), which is related to the trigonometric function of μ_{pre}. The right side of (12), which is the demand voltage-time area A_{de}, can be calculated using the predicted DC current. Hence, (12) is a transcendental equation of μ_{pre} that can be solved mathematically. However, the CF prediction and mitigation methods must be fast. Therefore, solving the transcendental equation might not be the best option.

The predicted OA μ_{pre} after the fault can be estimated using rated OA μ_{N}. As shown in Fig. 2, the area of curved trapezoid *ACDG* is approximately equal to the area of trapezoid *ACEG*. Therefore, A_{fact} can be replaced by $A_{\text{fact,appr}}$, which is an approximation of A_{fact}.

Meanwhile, at sample time t_{k}, *AG*, *BF*, and *AB* can be represented as:

$$\begin{cases} AG = E(\omega t_{\text{k}})\sin \alpha \\ BF = E(\omega t_{\text{k}})\sin(\alpha + \mu_{\text{N}}) \\ AB = \mu_{\text{N}} \end{cases} \qquad (13)$$

According to similarity theorem, *CE* can be calculated as:

$$CE = BF - \frac{\Delta\mu}{AB}(AG - BF) \qquad (14)$$

where $\Delta\mu = BC = \mu_{\text{pre}} - \mu_{\text{N}}$.

Hence, A_{fact} can be calculated as:

$$A_{\text{fact}} \approx A_{\text{fact, appr}} = \frac{1}{2}(AG + CE) \cdot AC \qquad (15)$$

Equation (15) can be rewritten as:

$$A_{\text{fact, appr}} = a(\Delta\mu)^2 + b\Delta\mu + c \qquad (16)$$

where $a = (BF - AG)/(2 \cdot AB)$; $b = BF$; and $c = AB \cdot (AG + BF)/2$.

Based on (11), A_{de} can be rewritten as:

$$A_{\text{de}} = X_{\text{c}}(I_{\text{dpre}}(\alpha) + I_{\text{dpre}}(\alpha + \mu_{\text{N}} + \Delta\mu)) \qquad (17)$$

where $I_{\text{dpre}}(\alpha) = I_{\text{d}}(\omega t_{\text{k}}) + [\alpha - \omega(t_{\text{k}} - t_0)]k_{I_{\text{d}}}(\omega t_{\text{k}})$; and $I_{\text{dpre}}(\alpha + \mu_{\text{N}} + \Delta\mu) = I_{\text{d}}(\omega t_{\text{k}}) + [\alpha + \mu_{\text{N}} + \Delta\mu - \omega(t_{\text{k}} - t_0)]k_{I_{\text{d}}}(\omega t_{\text{k}})$.

Substituting (10) into (17), we can obtain:

$$A_{\text{de}} = d\Delta\mu + e \qquad (18)$$

where $d = X_{\text{c}}k_{I_{\text{d}}}(\omega t_{\text{k}})$; and $e = X_{\text{c}}\{2I_{\text{d}}(\omega t_{\text{k}}) + [\mu_{\text{N}} + 2\alpha + 2\omega(t_0 - t_{\text{k}})]k_{I_{\text{d}}}(\omega t_{\text{k}})\}$.

$\Delta\mu$ can be solved using a quadratic equation formulated using (16) and (18). Hence, the predicted EA γ_{pre} can be expressed as:

$$\gamma_{\text{pre}} = \pi - \alpha - \mu_{\text{N}} - \Delta\mu \qquad (19)$$

Considering the phase shift in the commutation voltage $\Delta\varphi$, (19) can be rewritten as:

$$\gamma_{\text{pre}} = \pi - \alpha - \mu_{\text{N}} - \Delta\mu - \Delta\varphi \qquad (20)$$

In addition, for the fast and accurate prediction of CF, the predicted commutation margin is compared with the reference commutation margin $A_{\gamma_{\text{ref}}}$. Based on the rated RMS AC line-to-line voltage E_{ref} and reference EA γ_{ref}, the reference commutation margin for a successful commutation can be calculated as:

$$A_{\gamma_{\mathrm{ref}}} = \sqrt{2}\, E_{\mathrm{ref}} \int_{\pi-\gamma_{\mathrm{ref}}}^{\pi} \sin(\omega t)\omega t \, d(\omega t) = \sqrt{2}\, E_{\mathrm{ref}}(1-\cos\gamma_{\mathrm{ref}}) \quad (21)$$

The predicted commutation margin $A_{\gamma_{\mathrm{ref}}}$ can be calculated as:

$$A_{\gamma_{\mathrm{ref}}} = \sqrt{2}\, E(\omega t_{\mathrm{k}})(1-\cos\gamma_{\mathrm{pre}}) \quad (22)$$

The prediction of CF and the activation of the proposed FA control can be determined by comparing γ_{pre} and γ_{ref} or $A_{\gamma_{\mathrm{pre}}}$ and $A_{\gamma_{\mathrm{ref}}}$.

B. Prediction of FA

Since the change in the FA order affects the starting time of the commutation process and hence the values of A_{fact} and A_{de}, it is inaccurate to calculate the FA order based on merely μ_{pre} and γ_{ref}.

With the predicted FA α_{pre}, EA γ'_{pre} should be equal to γ_{ref} for a successful commutation and the lowest possible reactive power consumption. Figure 3 shows the prediction of advancing FA. The commutation voltage and the relationships among the predicted FA, OA, and EA with the predicted FA order at time t_{k} are also presented.
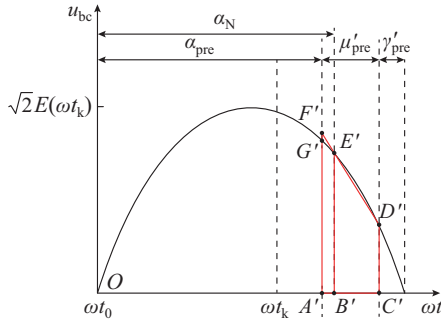

Fig. 3.   Prediction of advancing FA.

Substituting $\alpha_{\mathrm{pre}}+\mu'_{\mathrm{pre}}+\gamma'_{\mathrm{pre}}=\pi$ into (4), (23) can be expressed as:

$$\sqrt{2}\, E(\omega t_{\mathrm{k}})(\cos\alpha_{\mathrm{pre}}+\cos\gamma_{\mathrm{ref}})=X_{\mathrm{c}}(I_{\mathrm{dpre}}(\alpha_{\mathrm{pre}})+I_{\mathrm{dpre}}(\pi-\gamma_{\mathrm{ref}})) \quad (23)$$

Similar to (12), (23) is a transcendental equation of α_{pre} that can be solved mathematically. α_{pre} can be estimated using the rated FA α_{N}. As shown in Fig. 3, the area of curved trapezoid $A'C'D'G'$ is approximately equal to the area of trapezoid $A'C'D'F'$. Therefore, the predicted factual voltage-time area $A_{\mathrm{fact,pre}}$ can be replaced by $A_{\mathrm{fact,pre,appr}}$, which is an approximation of $A_{\mathrm{fact,pre}}$.

Since the RMS of AC line-to-line voltage is changed after a fault, γ'_{pre} is not exactly equal to γ_{ref}. Considering the effect of the RMS voltage on the turn-off time of the thyristor, γ'_{pre} can be calculated based on (24).

$$A_{\gamma_{\mathrm{ref}}} = \sqrt{2}\, E_{\mathrm{ref}}(1-\cos\gamma_{\mathrm{ref}}) = \sqrt{2}\, E(\omega t_{\mathrm{k}})(1-\cos\gamma'_{\mathrm{pre}}) \quad (24)$$

Solving (24) for γ'_{pre}, we can obtain:

$$\gamma'_{\mathrm{pre}} = \arccos\left(1 - \frac{E_{\mathrm{ref}}}{E(\omega t_{\mathrm{k}})} + \frac{E_{\mathrm{ref}}}{E(\omega t_{\mathrm{k}})}\cos\gamma_{\mathrm{ref}}\right) \quad (25)$$

Subsequently, $B'E'$, $C'D'$, and $A'B'$ can be represented as shown in (13) at sample time t_{k}.

$$\begin{cases} B'E'=E(\omega t_{\mathrm{k}})\sin\alpha_{\mathrm{N}} \\ C'D'=E(\omega t_{\mathrm{k}})\sin(\pi-\gamma'_{\mathrm{pre}}) \\ B'C'=\pi-\alpha_{\mathrm{N}}-\gamma'_{\mathrm{pre}} \end{cases} \quad (26)$$

According to similarity theorem, $A'F'$ can be calculated as:

$$A'F'=B'E'+\frac{\Delta\alpha}{B'C'}(B'E'-C'D') \quad (27)$$

where $A'B'=\Delta\alpha=\alpha_{\mathrm{N}}-\alpha_{\mathrm{pre}}$.

Therefore, $A_{\mathrm{fact,pre}}$ can be calculated as:

$$A_{\mathrm{fact,pre}} \approx A_{\mathrm{fact,pre,appr}} = \frac{1}{2}(A'F'+C'D')\cdot A'C' \quad (28)$$

Equation (28) can be rewritten as:

$$A_{\mathrm{fact,pre,appr}} = a'(\Delta\alpha)^2 + b'\Delta\alpha + c' \quad (29)$$

where $a'=(B'E'-C'D')/(2\cdot B'C')$; $b'=B'E'$; and $c'=B'C'\cdot(B'E'+C'D')/2$.

Based on (23), $A_{\mathrm{de,pre}}$ can be rewritten as:

$$A_{\mathrm{de,pre}}=X_{\mathrm{c}}(I_{\mathrm{dpre}}(\alpha_{\mathrm{N}}-\Delta\alpha)+I_{\mathrm{dpre}}(\pi-\gamma'_{\mathrm{pre}})) \quad (30)$$

Similar to (17), substituting (10) into (30), we can obtain:

$$A_{\mathrm{de,pre}}=d'\Delta\alpha+e' \quad (31)$$

where $d'=X_{\mathrm{c}}k_{I_{\mathrm{d}}}(\omega t_{\mathrm{k}})$; and $e'=X_{\mathrm{c}}\{2I_{\mathrm{d}}(\omega t_{\mathrm{k}})+[\pi-\gamma'_{\mathrm{pre}}+2\omega(t_0-t_{\mathrm{k}})]k_{I_{\mathrm{d}}}(\omega t_{\mathrm{k}})\}$. $\Delta\alpha$ can be solved using a quadratic equation formulated using (29) and (31). Hence, α_{pre} can be calculated as:

$$\alpha_{\mathrm{pre}}=\alpha_{\mathrm{N}}-\Delta\alpha \quad (32)$$

Considering the phase shift in the commutation voltage $\Delta\varphi$, (32) can be rewritten as:

$$\alpha_{\mathrm{pre}}=\alpha_{\mathrm{N}}-\Delta\alpha-\Delta\varphi \quad (33)$$

C. Proposed CF Prediction and Mitigation Method

A two-terminal HVDC system comprises a rectifier side and an inverter side, each of which has its own control system. Figure 4 shows the block diagram of the proposed method. Under normal conditions, the constant extinction angle (CEA) controller is used to regulate the DC voltage and ensure a minimum value of the EA to maintain a low reactive power consumption. Under fault conditions, the current error controller (CEC) is used to switch the control mode from the CEA to the constant current (CC) controller, and the rectifier is operated in the minimum α mode. The VDCOL contributes to the recovery of the LCC-HVDC system by increasing the DC current gradually after fault clearance.

The inverter control system is equipped with the proposed method for CF prediction and mitigation because the risk of CF at the inverter side is higher than that at the rectifier side. The flowchart of the proposed method is shown in Fig. 5, and the detailed procedure of the proposed method is described as follows.

1) For any commutation process, the EA is predicted because the commutation voltage changes from a negative value to a positive one. The RMS AC line-to-line voltage is calculated using second-order general integrator (SOGI) [27]. The DC current $I_{\mathrm{d}}(\omega t_{\mathrm{k}})$ is calculated using a moving average filter [28], and the rate of DC current $k_{I_{\mathrm{d}}}(\omega t_{\mathrm{k}})$ is the first-order derivative of $I_{\mathrm{d}}(\omega t_{\mathrm{k}})$.
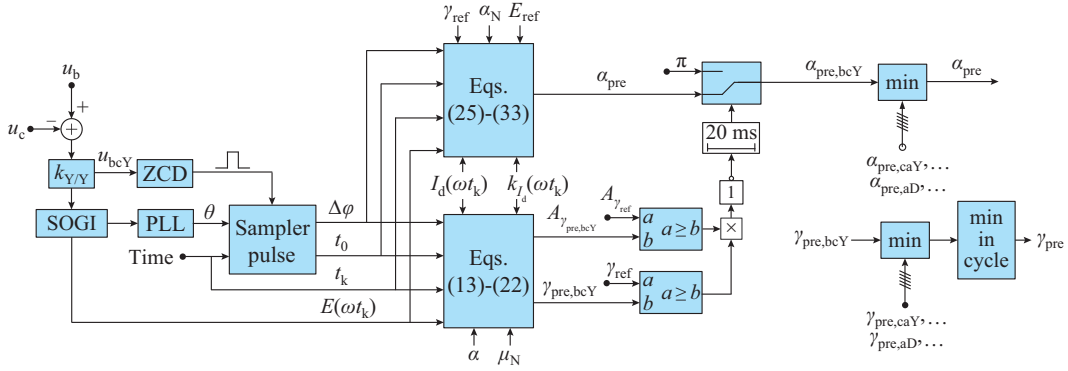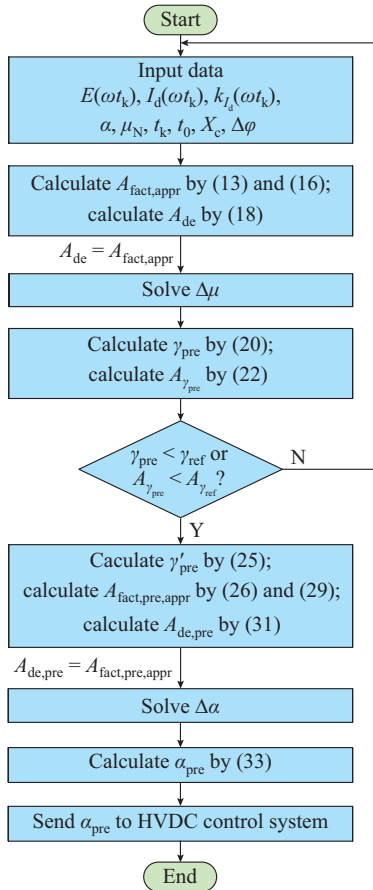
Fig. 4. Block diagram of proposed method.

Fig. 5. Flowchart of proposed method.

Meanwhile, $\Delta\varphi$ is calculated based on the output phase angle θ of the phase-locked loop (PLL) at t_0, which is detected by the zero-crossing detector (ZCD). γ_{pre} and $A_{\gamma_{pre}}$ are calculated using (13)-(20) and (22), respectively. Under normal conditions, γ_{pre} and $A_{\gamma_{pre}}$ remain unchanged. In the case of AC faults, γ_{pre} and $A_{\gamma_{pre}}$ decrease because of voltage drop, DC current increase, and phase shift. If $\gamma_{pre} < \gamma_{ref}$ or $A_{\gamma_{pre}} < A_{\gamma_{ref}}$, then the trigger signal is sent to the selector, thereby enabling the proposed FA control. In particular, the trigger signal is extended to 20 ms to improve the performance of CF mitigation. To avoid unnecessary fluctuations caused by the action of the proposed control and to enable the proposed control

quickly under fault conditions, γ_{ref} is selected as 10°.

2) The predicted FA $\alpha_{pre, i}$ ($i =$ aD, bD, cD, abY, bcY, caY) of any commutation process can be calculated using (25)-(33), and the minimum calculated value among all results is considered as α_{pre}. The FA order α_{ord} of the inverter valves is the smaller value between α_{pre} and the FA α of CIGRE.

IV. SIMULATION AND RESULTS

A. Test Model

To validate the effectiveness of the proposed method, several simulations are performed using the CIGRE benchmark HVDC model based on PSCAD/EMTDC. The parameters of the test network are listed in Table I. CFPREV control strategy [22] is developed in PSCAD/EMTDC for comparison with the proposed method, which is explained comprehensively in Appendix A.

TABLE I
PARAMETERS OF TEST NETWORK

Item	Rectifier side	Inverter side
AC voltage	382.87 kV	215.05 kV
SCR	2.5	2.5
Reactive compensation	626 Mvar	626 Mvar
Transformer ratio	345 kV/213.5 kV	230 kV/209.2 kV
Transformer leakage inductance	0.18 p.u.	0.18 p.u.
Reactive compensation	626 Mvar	626 Mvar
DC resistance	5 Ω	5 Ω
DC inductance	1.2 H	1.2 H
Rated DC voltage	500 kV	500 kV
Rated DC current	2 kA	2 kA

B. Performance of Proposed EA Prediction Method

Figure 6 shows the performance of the proposed EA prediction method with single-phase line-to-ground (A-G) and three-phase line-to-ground (ABC-G) AC faults with different fault inductances L_f and fault resistances R_f. In all cases, the fault is applied at $t = 3.0$ s for a duration of 0.05 s.

As shown in Fig. 6, in contrast to the step change in the measured EA, the predicted EA changes gradually with the related electric quantities such as the DC current and the RMS of the commutation voltage. During the fault, the varia-

tion tendency of the predicted EA is consistent with that of the measured EA. Moreover, the predicted EA changes quickly and earlier than the measured EA, thereby enabling the CF to be predicted in advance rather than detecting the CF after its occurrence. The proposed method is more accurate and sensitive to resistance grounding faults and severe faults. Owing to the measurement delay and phase-locked error, a prediction error is inevitable. In particular, with a slight fault when the DC current increases slowly, the demand $A_{\mathrm{de,pre}}$ is less than the actual value, resulting in a smaller $\Delta\mu$ and a larger γ_{pre}.
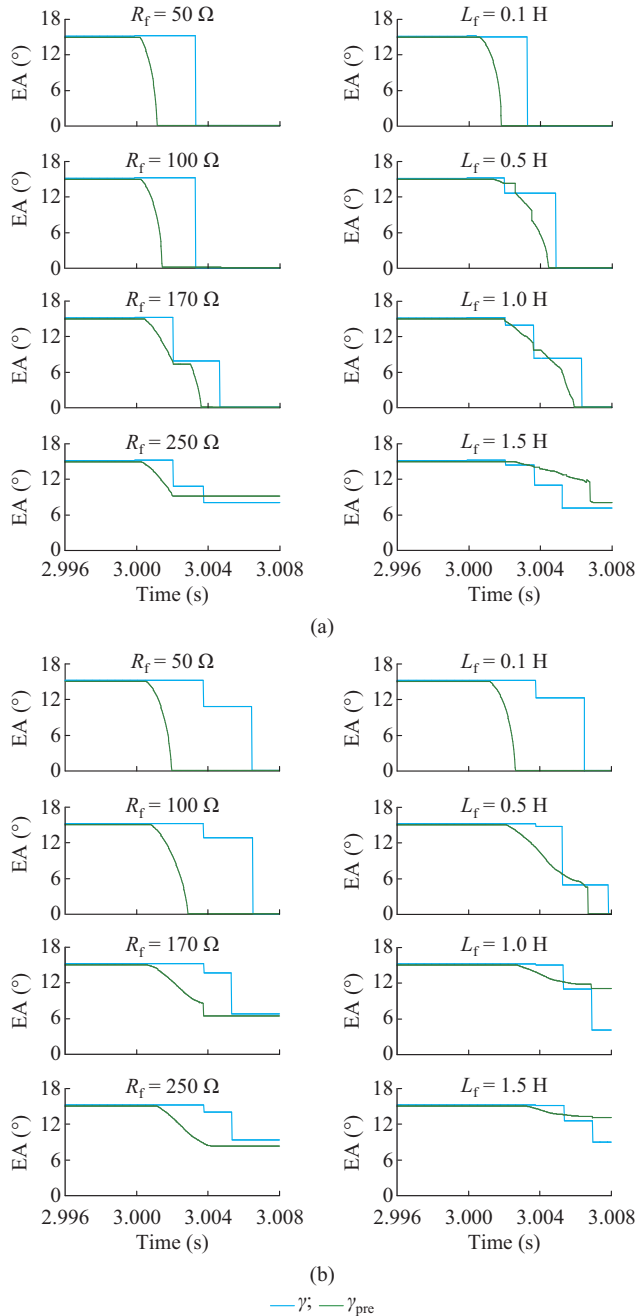

Fig. 6. Comparison of predicted EA γ_{pre} and measured EA γ with different faults. (a) A-G AC faults with different L_f and R_f. (b) ABC-G AC faults with different L_f and R_f.

When the fault is not severe, CF might still occur, particu-

larly with an inductance grounding fault. The proposed method is quickly activated through a comparison between $A_{\gamma_{\mathrm{pre}}}$ and $A_{\gamma_{\mathrm{ref}}}$. The performances of the proposed method with A-G and ABC-G AC faults with different L_f at 3.0 s are presented in Table II. As shown in Table II, the proposed method can activate the proposed FA control quickly. Similarly, when faults are applied at other time, the proposed method can react quickly. Although the FA control acts unnecessarily with some faults, the fluctuation is slight with the action of the proposed method.

TABLE II
PERFORMANCES OF PROPOSED METHOD

Fault type	L_f (H)	Action time (s)	CF prediction time (s)	CF time (s)
A-G	0.1	3.0021	3.0026	3.0065
	0.5	3.0037	3.0066	3.0078
	1.0	3.0059		
	1.5			
ABC-G	0.1	3.0012	3.0018	3.0033
	0.5	3.0025	3.0043	3.0049
	1.0	3.0031	3.0058	3.0063
	1.5	3.0065		

C. Performance of Proposed FA Control in Terms of CF Mitigation

A-G and ABC-G AC faults are applied in a typical case to verify the effectiveness of the proposed method in terms of CF mitigation. With different L_f, the faults are applied on the inverter-side AC bus to simulate different fault severity levels. In all cases, the faults are applied from 3.000 to 3.009 s at a step size of 0.001 s for a duration of 0.05 s.

1) A-G AC fault simulation: L_f varies from 0.56 H to 0.9 H. With the decrease in L_f, the fault location is closer to the AC bus, i.e., the fault is more severe. Figure 7(a) shows the A-G AC fault test results and the proposed method performs better in mitigating CF. However, at some fault time such as 3.004 s, the effect of the proposed method is limited. This is because the ability to mitigate CF depends on the commutation process of valve 1 to valve 3 and valve 4 to valve 6 with A-G AC faults. When the fault time is far from the time at which commutation occurs at valve 1 to valve 3 and valve 4 to valve 6, the system has sufficient time to adjust to mitigate CF. Hence, either CFPREV or the proposed method is effective in this situation.

Figure 8(a) shows the simulation results when the A-G AC fault is applied at 3.000 s and L_f is 0.7 H. When an A-G AC fault occurs at the inverter-side AC bus, the risk of CF increases with the joint action of the voltage drop and DC increase. In the CIGRE control, the measured EA is updated when the commutation voltage crosses zero, resulting in a distinct delay in the CIGRE control. As indicated by the blue lines in Fig. 8(a), CF occurs, the DC voltage decreases significantly, and the DC current increases to 2.4 p.u.. The proposed method is applied to mitigate CF.
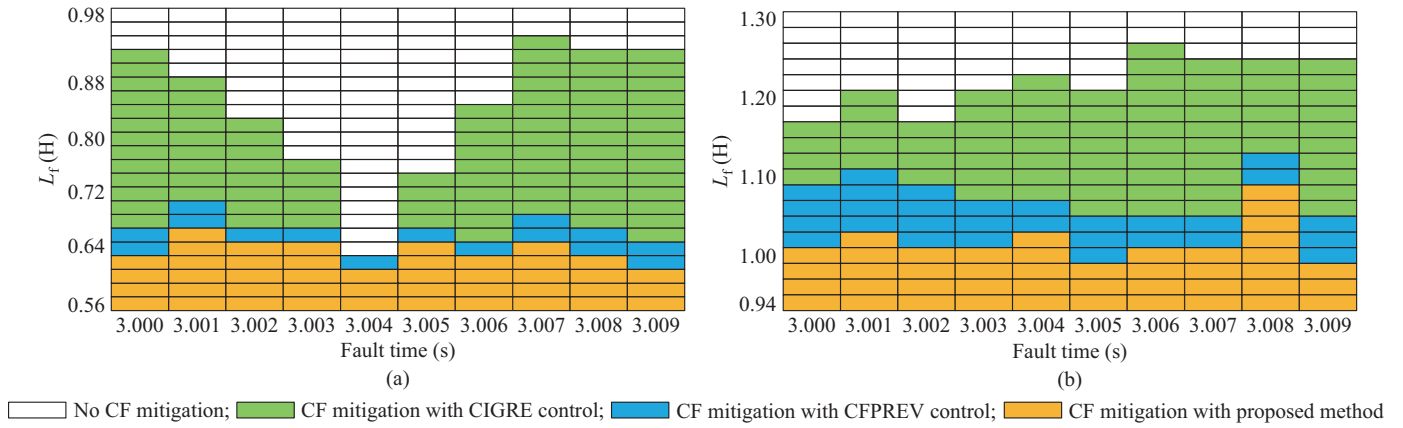
Fig. 7.　Performance of CF mitigation with different controls. (a) A-G AC faults. (b) ABC-G AC faults.
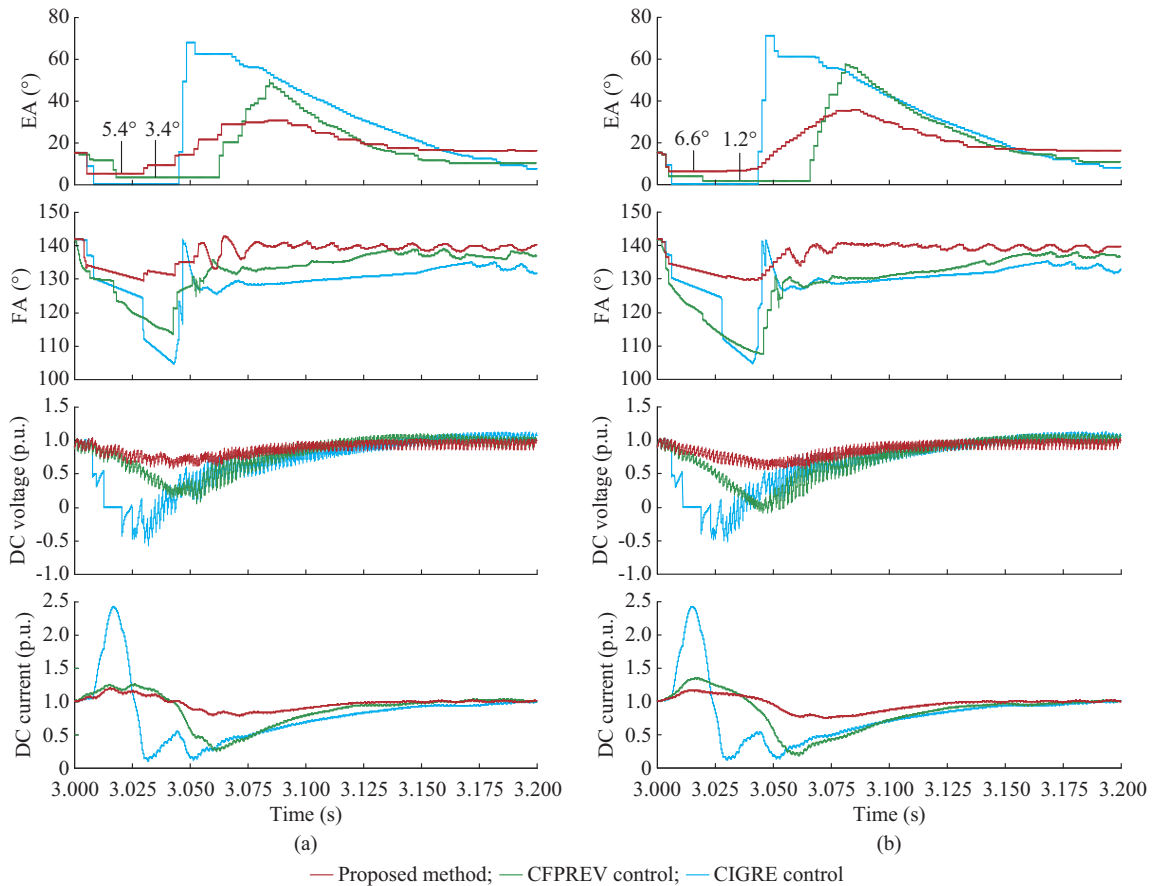

Fig. 8.　System response with different controls. (a) A-G AC fault. (b) ABC-G AC fault.

As indicated by the red lines in Fig. 8(a), the minimum EA after the fault is 5.4°, which implies that CF can be avoided. As indicated by the green lines in Fig. 8(a), CF-PREV control is applied and CF is avoided. However, it is noteworthy that the minimum EA after the fault is 3.4°, which is 2.0° less than that of the proposed method. As indicated by the green lines in Fig. 8(a), the FA order continues to decrease even when the EA exceeds 10°, thereby resulting in an increase in the DC current and a greater consumption of reactive power, causing the AC voltage to decrease further and the output of CFPREV control to increase consequently. Finally, the EA decreases to 3.4°. Moreover, the pro-

posed method can mitigate CF with a larger FA, which implies a lower reactive power consumption. In addition, fluctuations in the DC current and DC voltage are less significant when the proposed method is used, which implies that the system applying the proposed method is affected less by the fault compared with the system with CIGRE control or CF-PREV control.

2) ABC-G AC fault simulation: L_f varies from 0.94 H to 1.3 H. The same analysis can be extended to ABC-G AC faults, as shown in Figs. 7(b) and 8(b). Figure 7(b) shows that the proposed method performs better in mitigating CF compared with the CIGRE control or CFPREV control. How-

ever, at some sensitive fault time such as 3.008 s, the effect of the proposed method is inconspicuous. This is because the commutation process starts immediately or is ongoing at that time. Figure 8(b) shows the simulation results when the ABC-G AC fault is applied at 3.000 s, and L_f is 1.1 H. As shown in Fig. 8(b), the CF could not be avoided when CIGRE control is applied. Using the proposed method, the minimum EA after the fault is 6.6°, which is 5.4° higher than that of the CFPREV control. The fluctuation is less significant when the proposed method is used in this case. Therefore, it can be concluded that the proposed method performs better in terms of CF mitigation than the other two controls.

V. CONCLUSION

A method for CF prediction and mitigation is proposed based on the boundary condition of the commutation process and a prediction of the DC current. By analyzing the simulation results of the CIGRE benchmark HVDC model built in PSCAD/EMTDC, the following can be concluded.

1) The proposed method can predict CF rapidly and activate the CF mitigation method after the occurrence of faults. The EA prediction method is more sensitive and accurate for resistance grounding faults and severe faults.

2) The proposed method can improve the CF mitigation capability of the system with A-G and ABC-G AC faults.

3) The proposed method performs better in terms of CF mitigation without requiring parameter tuning.

APPENDIX A

The improved CFPREV [29] based on the original CFPREV [22] is adopted. It deducts $\Delta\alpha$ from FA order α based on the fault severity (voltage drop severity) to prevent CF:

$$\Delta\alpha = \arccos\left(1 - \max\left(k_1\left|U_0\right|, k_2\Delta U_{\alpha\beta}, k_3\Delta U_{i\max}\right)\right)$$

where k_1, k_2, and k_3 are the proportional coefficients; and U_0, $U_{\alpha\beta}$, and U_i are the zero-sequence voltage, rotating vector magnitude, and single-phase voltage amplitude calculated by using sine-cosine components [30], respectively.

Although the reaction of CFPREV may be unnecessary, $U_{0,\text{level}}$, $U_{\alpha\beta,\text{level}}$, and $U_{i,\text{level}}$ are set to be relatively small values to fulfill the potential of CFPREV. The parameters of the CFPREV are listed in Table AI.

TABLE AI
PARAMETERS OF CFPREV

Parameter	Value
$U_{0,\text{level}}$	0.00108 p.u.
k_1	0.225
$U_{i,\text{level}}$	0.00054 p.u.
k_3	0.075
$U_{\alpha\beta,\text{level}}$	0.027 p.u.
k_2	0.075

REFERENCES

[1] D. Kwon, Y. J. Kim, and S. I. Moon, "Modeling and analysis of an LCC HVDC system using DC voltage control to improve transient response and short-term power transfer capability," *IEEE Transactions on Power Delivery*, vol. 33, no. 4, pp. 1922-1933, Aug. 2018.

[2] J. Wu, H. Li, G. Wang et al., "An improved traveling-wave protection scheme for LCC-HVDC transmission lines," *IEEE Transactions on Power Delivery*, vol. 32, no. 1, pp. 106-116, Feb. 2017.

[3] T. Wu, Y. Zheng, Q. Liu et al., "Continuous commutation failure suppression method based on self-adaptive auto-disturbance rejection proportional-integral controller for HVDC transmission system," *Journal of Modern Power Systems and Clean Energy*, vol. 8, no. 6, pp. 1178-1187, Nov. 2020.

[4] C. Guo, Y. Zhang, A. M. Gole et al., "Analysis of dual-infeed HVDC with LCC HVDC and VSC HVDC," *IEEE Transactions on Power Delivery*, vol. 27, no. 3, pp. 1529-1537, Jul. 2012.

[5] Q. Tao and Y. Xue, "Quantitative assessment for commutation security based on extinction angle trajectory," *Journal of Modern Power Systems and Clean Energy*, vol. 9, no. 2, pp. 328-337, Mar. 2021.

[6] H. Xiao, Y. Li, J. Zhu et al., "Efficient approach to quantify commutation failure immunity levels in multi-infeed HVDC systems," *IET Generation, Transmission & Distribution*, vol. 10, no. 4, pp. 1032-1038, Oct. 2015.

[7] J. Arrillaga, *High Voltage Direct Current Transmission*. London: Institution of Electrical Engineers, 1998.

[8] M. Jafar and M. Molinas, "Ride-through enhancement of line-commutated HVDC link for large offshore wind parks," in *Proceedings of IEEE Industrial Electronics Conference*, Porto, Portugal, Nov. 2009, pp. 782-787.

[9] J. Zhang, W. Jiang, Y. Yin et al., "Security and stability study on planned ultra high voltage power grid," *Proceedings of the CSEE*, vol. 28, no. 22, pp. 64-68, Aug. 2008.

[10] Y. Sun, L. Peng, F. Ma et al., "Design a fuzzy controller to minimize the effect of HVDC commutation failure on power system," *IEEE Transactions on Power Systems*, vol. 23, no. 1, pp. 100-107, Feb. 2008.

[11] F. Wang, T. Liu, and X. Li, "Decreasing the frequency of HVDC commutation failures caused by harmonics," *IET Power Electronics*, vol. 10, no. 2, pp. 215-221, Oct. 2017.

[12] S. Gomes, N. Martins, T. Jonsson et al., "Modeling capacitor commutated converters in power system stability studies," *IEEE Transactions on Power Systems*, vol. 17, no. 2, pp. 371-377, May 2002.

[13] S. Zhou, J. Wu, W. Cao et al., "Study on transient characteristics of CCC-HVDC transmission systems," in *Proceedings of International Conference on Sustainable Power Generation and Supply*, Hangzhou, China, Sept. 2012, pp. 1-5.

[14] K. Sadek, M. Pereira, D. P. Brandt et al., "Capacitor commutated converter circuit configurations for DC transmission," *IEEE Transactions on Power Delivery*, vol. 13, no. 4, pp. 1257-1264, Oct. 1998.

[15] C. Guo, C. Li, C. Zhao et al., "An evolutional line commutated converter integrated with thyristor based full-bridge module to mitigate the commutation failure," *IEEE Transactions on Power Electronics*, vol. 32, no. 2, pp. 967-976, Feb. 2016.

[16] O. B. Nayak, A. M. Gole, D. G. Chapman et al., "Dynamic performance of static and synchronous compensators at an HVDC inverter bus in a very weak AC system," *IEEE Transactions on Power Systems*, vol. 9, no. 3, pp. 1350-1358, Aug. 1994.

[17] C. Zhao, D. Li, Y. Liu et al., "Control method for HVDC system with STATCOM," *High Voltage Engineering*, vol. 40, no. 8, pp. 2440-2448, Aug. 2014.

[18] C. Li, C. Zhao, Y. Liu et al., "Analysis and design of topological structure for a new HVDC current limiter," *Power Systems Technology*, vol. 39, no. 7, pp. 1819-1824, Jul. 2015.

[19] S. Mirsaeidi, X. Dong, D. Said et al., "A fault current limiting approach for commutation failure prevention in LCC-HVDC transmission systems," *IEEE Transactions on Power Delivery*, vol. 34, no. 5, pp. 2018-2027, Oct. 2019.

[20] M. Nguyen, T. Saha, and M. Eghbal, "Master self-tuning VDCOL function for hybrid multi-terminal HVDC connecting renewable resources to a large power system," *IET Generation, Transmission & Distribution*, vol. 11, no. 1, pp. 3341-3349, Jul. 2017.

[21] Q. Meng, Z. Hong, L. Rong et al., "A suppression method based on nonlinear VDCOL to mitigate the continuous commutation failure," *Power System Protection and Control*, vol. 47, no. 7, pp. 119-127, Apr. 2019.

[22] L. Zhang and L. Dofnas, "A novel method to mitigate commutation failures in HVDC systems," in *Proceedings of International Conference on Power System Technology*, Kunming, China, Oct. 2002, pp. 51-56.

[23] J. Wang, Z. Wang, X. Xuan et al., "Extinction angle control based on predictive calculation and its improvement," *Power System Technolo-

gy, vol. 42, no. 12, pp. 3985-3991, Dec. 2018.

[24] Z. Wei, Y. Yuan, X. Lei *et al.*, "Direct-current predictive control strategy for inhibiting commutation failure in HVDC converter," *IEEE Transactions on Power Systems*, vol. 29, no. 5, pp. 2409-2417, Sept. 2014.

[25] S. Mirsaeidi and X. Dong. "An enhanced strategy to inhibit commutation failure in line-commutated converters," *IEEE Transactions on Industrial Electronics*, vol. 67, no. 1, pp. 340-349, Jan. 2020.

[26] L. Liu, S. Lin, P. Sun *et al.*, "A calculation method of pseudo extinction angle for commutation failure mitigation in HVDC," *IEEE Transactions on Power Delivery*, vol. 34, no. 2, pp. 777-779, Apr. 2019.

[27] M. Ciobotaru, R. Teodorescu, and F. Blaabjerg, "A new single-phase PLL structure based on second order generalized integrator," in *Proceedings of IEEE Power Electronics Specialists Conference (PESC'06)*, Jeju, Korea, Jun. 2006, pp. 1-6.

[28] S. Golestan, M. Ramezani, J. M. Guerrero *et al.*, "Moving average filter based phase-locked loops: performance analysis and design guidelines," *IEEE Transactions on Power Electronics*, vol. 29, no. 6, pp. 2750-2763, Jun. 2014.

[29] S. Chen, X. Li, and J. Yu, "Method based on the sin-cos components detection mitigates commutation failure in HVDC," *Proceedings of the CSEE*, vol. 25, no. 14, pp. 1-6, Jul. 2005.

[30] S. Tamai, H. Naitoh, F. Ishiguro *et al.*, "Fast and predictive HVDC extinction angle control," *IEEE Transactions on Power Systems*, vol. 12, no. 3, pp. 1268-1275, Aug. 1997.

Renlong Zhu received the B.Eng. degree from the College of Electrical and Information Engineering, Hunan University, Changsha, China, in 2018. He is currently pursuing her Ph.D. degree in electrical engineering in the College of Electrical and Information Engineering, Hunan University since 2020. His research interests include modeling and control of LCC-HVDC and VSC-HVDC.

Xiaoping Zhou received the B.Eng., M.S., and Ph. D. degrees from the College of Electrical and Information Engineering, Hunan University, Changsha, China, in 2009, 2013, and 2018, respectively. Currently, he is a full-time Associate Professor in electrical engineering at Hunan University. His research interests include HVDC, power electronics, distributed generation, microgrid, power quality and energy storage.

Haitao Xia received the B.Eng. degree from the College of Electrical and Information Engineering, Hunan University, Changsha, China, in 2017. He is currently pursuing her Ph.D. degree in electrical engineering in the College of Electrical and Information Engineering, Hunan University, since 2019. His research interests include HVDC and dynamic analysis of power electronics converter.

Lerong Hong received the B. Eng. degree from the College of Electrical and Information Engineering, Hunan University, Changsha, China, in 2016. He is currently pursuing her Ph.D. degree in electrical engineering in the College of Electrical and Information Engineering, Hunan University, since 2017. His research interests include HVDC and power electronic converter.

Hanhang Yin received the B. Eng. degree from the College of Electrical and Information Engineering, Hunan University, Changsha, China, in 2018. She is currently pursuing her Ph.D. degree in electrical engineering in the College of Electrical and Information Engineering, Hunan University, since 2020. Her research interests include power electronic converter modeling, stability analysis, and modular multilevel converter.